Design and Fabrication of a Band-Pass Filter With EBG Single-Ridge Waveguide Using Additive Manufacturing Techniques

Héctor García-Martínez, Ernesto Ávila-Navarro, Germán Torregrosa-Penalva, *Member, IEEE*, Nicolò Delmonte, *Student Member, IEEE*, Lorenzo Silvestri, *Member, IEEE*, Stefania Marconi, Gianluca Alaimo, Ferdinando Auricchio, and Maurizio Bozzi, *Fellow, IEEE*

***Abstract*— A novel band-pass filter topology in waveguide technology is presented in this work. The proposed filter design is based on a periodic structure that uses modified sections of a single-ridge waveguide (SRW) as the unit cell to produce the desired frequency response. Two-step height profiles are included in the central part of the SRW, which provide useful parameters to yield a simple design method to achieve the required filtering characteristics. The suggested topology and design process are used to achieve band-pass filter responses with different fractional bandwidth and rejection characteristics. A 54% fractional bandwidth band-pass filter centered at 5.4 GHz is implemented using low cost 3-D additive manufacturing techniques, which allow fast prototyping and the fabrication of complex geometries. Experimental measurements are in agreement with the expected simulated response of the designed band-pass filter.**

***Index Terms*— 3-D printing, additive manufacturing, bandgap, microwave filter, single-ridge waveguide (SRW).**

I. Introduction

ADDITIVE manufacturing techniques and 3-D printers are currently arousing great interest in a wide variety of fields such as medicine and science and technology [1]. Nowadays, commercial 3-D printers combine low cost with high precision, allowing a large number of degrees of freedom for the end user. One of the most interesting features of 3-D printing is the suitability to perform devices with complex geometries [2], [3], which are not feasible with current milling machines, based on subtractive material technologies. Due to these characteristics, 3-D printing techniques are being widely used in recent years to develop microwave devices in different technologies such as waveguide technology, substrate integrated waveguide (SIW), and planar circuits [4]–[8].

On the other hand, periodic structures show very attractive properties in the frequency domain associated with their electromagnetic bandgap (EBG) characteristics, such as greater out-of-band rejection and reduced size, which makes them possible candidates for being used in filtering applications at microwave and millimeter-wave frequencies [9]. Recently, a new filter topology in rectangular waveguide technology has been introduced [10], where variations in the height of the rectangular waveguide allow to modify the impedance of the waveguide, thus creating sections with different wave impedance values. Similar developments of this kind of filters have been reported in [11]–[13], adding flexibility to the design and extending this concept to SIW structures.

In this work, a new band-pass filter topology is presented, where single-ridge waveguide (SRW) technology is used, following a similar concept as in [10], to implement periodic structures and achieve EBG characteristics. The SRW technology is used to move the cutoff frequency of the second mode of the waveguide to higher frequencies [14]–[16], so that wider single-mode bandwidths are obtained allowing the design of wider fractional bandwidth band-pass filters. This is accomplished by adding impedance variations in the central section in the direction of propagation of the SRW waveguide. The implementation of the proposed filter topology is not evident making use of conventional fabrication techniques, which is why, in our work, this implementation is done by means of 3-D additive manufacturing techniques.

This article is organized as follows. In Section II, the electromagnetic analysis of the SRW waveguide is carried out through the dispersion diagram of the Floquet modes of the infinite periodic structure, providing the allowed and prohibited frequency bands of the structure for different design parameters. Section III is first dedicated to the study of the finite EBG waveguide. In this section, two filter designs with

Manuscript received March 4, 2020; revised May 18, 2020 and June 12, 2020; accepted June 21, 2020. Date of publication July 15, 2020; date of current version October 5, 2020. This work was supported by the Agencia Estatal de Investigación (AEI) and EU through the Fondo Europeo de Desarrollo Regional (FEDER)-"A way to build Europe" under Grant DPI2016-80391-C3-2-R [AEI/FEDER, UE]. *(Corresponding author: Héctor García-Martínez.)*

Héctor García-Martínez and Ernesto Ávila-Navarro are with the Department of Materials Science, Optical and Electronic Technology, University Miguel Hernández of Elche, 03202 Elche, Spain (e-mail: mhector@umh.es; eavila@umh.es).

Germán Torregrosa-Penalva is with the Communication Engineering Department, University Miguel Hernández of Elche, 03202 Elche, Spain (e-mail: gtorregrosa@umh.es).

Nicolò Delmonte, Lorenzo Silvestri, and Maurizio Bozzi, are with the Department of Electrical, Computer, and Biomedical Engineering, University of Pavia, 27100 Pavia, Italy (e-mail: nicolo.delmonte01@universitadipavia.it; lorenzo.silvestr-i01@universitadipavia.it; maurizio.bozzi@unipv.it).

Stefania Marconi, Gianluca Alaimo, and Ferdinando Auricchio are with the Department of Civil Engineering and Architecture, University of Pavia, 27100 Pavia, Italy (e-mail: stefaniamarconi@unipv.it; gianluca.alaimo01@universitadipavia.it; auricchio@unipv.it).

Color versions of one or more of the figures in this article are available online at http://ieeexplore.ieee.org.

Digital Object Identifier 10.1109/TMTT.2020.3006836

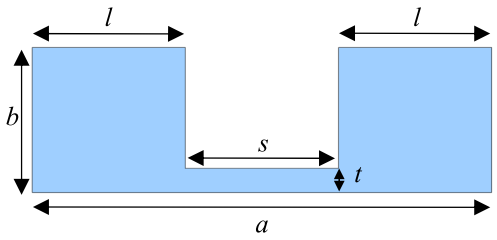

Fig. 1. Cross section of the SRW with design parameters.

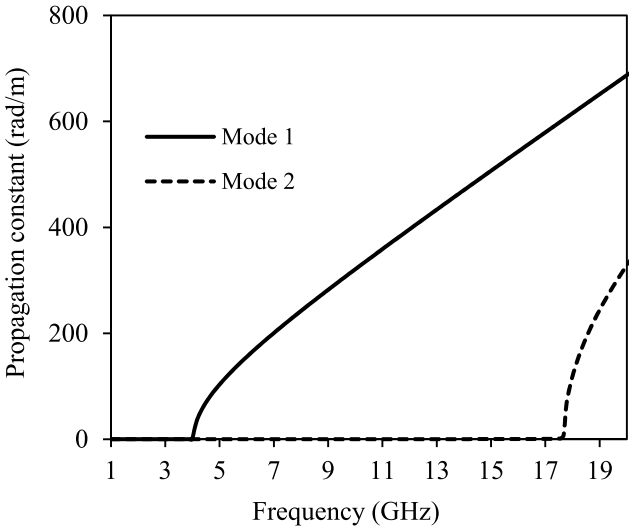

Fig. 2. Simulated propagation constants of the first two modes in the SRW.

different fractional bandwidths are presented, and finally one of them is fabricated. Section IV describes the manufacturing and measurement process of the implemented filter, and some final conclusions of this work are given in Section V.

II. Study of the Unit Cell

Periodic waveguides are a particular case of EBG structures, which have a unidimensional periodic pattern in the direction of the signal propagation [9]. Then, it is possible to obtain bandgap frequencies where the signal cannot propagate. In this section, an SRW structure as a periodic unit cell is studied. The unit cell includes in the middle of the waveguide a step to achieve a prohibited bandgap for the fundamental mode.

It is well-known that a periodic waveguide structure presents pass bands and rejection bands in the frequency domain associated with the dispersion of the Floquet modes [17], [18], which are the solutions of Maxwell's equations in this type of periodic structure. The frequency bands in which at least one Floquet mode is propagated provide the different pass bands of the periodic structure. On the contrary, the rejection bands are characterized by the absence of propagation of the Floquet modes. Therefore, to characterize the behavior of the periodic structure in a given frequency range, the dispersion or Brillouin diagram of the different Floquet modes in the periodic structure must be calculated. This can be achieved in different ways, depending on the dimensions of the waveguide under study. In this work, the eigenmode solver of the commercial electromagnetic software Ansys HFSS [19], [20] has been used.

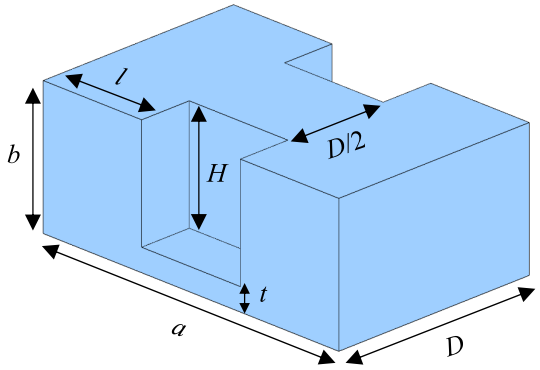

Fig. 3. EBG SRW unit cell.

A. Design and Simulation of the SRW

To design the SRW shown in Fig. 1, a cutoff frequency of $f_1 = 4$ GHz has been selected [14], [21]. The optimized final dimensions of the SRW are $a = 10$ mm, $b = 3.78$ mm, $t = 0.63$ mm, and $l = s = 3.33$ mm. The material used to implement the waveguide is a low-cost 3-D printing filament of natural polylactic acid (PLA) with a diameter of 1.75 mm, and its measured characteristics are as follows: relative dielectric permittivity constant $\varepsilon_r = 2.8$ and loss tangent $\tan\delta = 0.02$, [10], [22]. The metallic layers are implemented using copper. Fig. 2 shows the propagation constant for the first two modes of the designed SRW. The respective cutoff frequencies are $f_1 = 4$ GHz and $f_2 = 17.5$ GHz, leading to a single-mode bandwidth factor of $B = 3$, where B is defined in [17] as

$$B = \frac{f_2 - f_1}{f_1}. \tag{1}$$

B. Analysis of the Unit Cell in the Periodic Structure

Hereafter, a unit periodic cell of the previously designed SRW is studied, including in the central waveguide part a two-step section as shown in Fig. 3. The propagation constants of the modes in the structure are modified by the inclusion of this step, depending not only on the SRW design parameters but also on the step dimensions. To maintain a cutoff frequency of $f_1 = 4$ GHz for the first mode, the dimensions transversal to the direction of propagation are recalculated using the electromagnetic software HFSS increased by a factor of 1.16.

The period of the unit cell can be determined as in [9] and [10] by

$$D = \frac{\lambda_g}{4} \tag{2}$$

where λ_g is the guided wavelength at the central frequency of the bandgap. In this case, the bandgap has been selected at a central frequency of 7 GHz to act directly on the fundamental mode.

The final dimensions of the designed unit cell are as follows: $a = 11.65$ mm, $b = 3.78$ mm, $t = 0.63$ mm, y $l = s = 3.88$ mm, $H = 3.15$ mm, and $D = 15$ mm. Fig. 4 shows the dispersion diagram of the first five Floquet modes of the structure. Their cutoff frequencies are $f_1 = 4$ GHz,

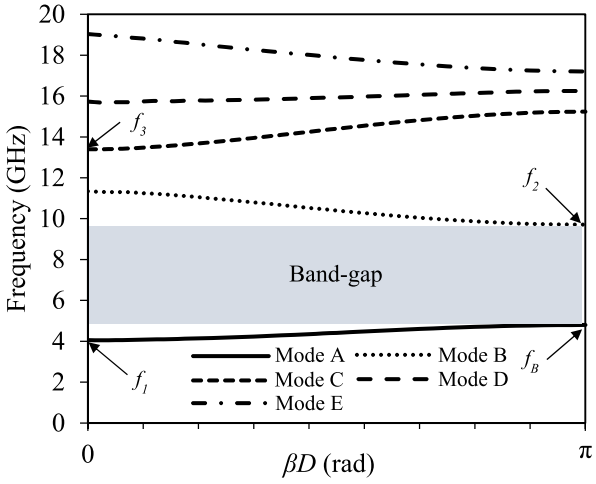

Fig. 4. Dispersion diagram of the periodic structure.

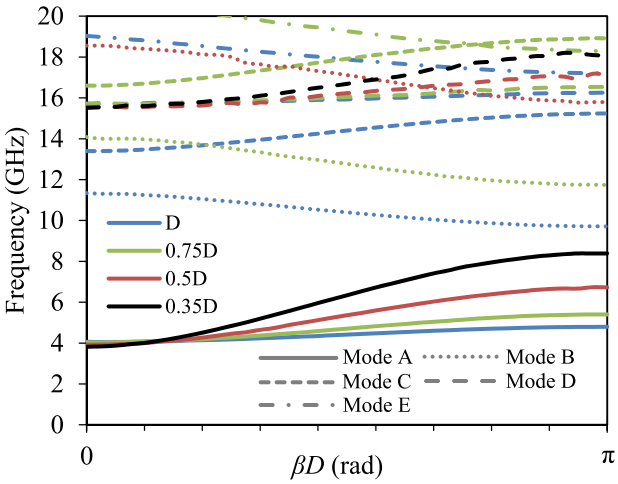

Fig. 5. Dispersion diagram of the EBG SRW for a step height H and different period lengths of the unit cell.

$f_2 = 9.8$ GHz, and $f_3 = 13.8$ GHz, while the designed bandgap is as desired centered around 7 GHz, which yields $B = 1.42$. A passband bandwidth is defined between the cutoff frequency of the fundamental mode f_1 and the lowest frequency of the band-gap f_B, which allows to calculate a fractional passband bandwidth of $\Delta = 17.8\%$ using

$$\Delta = \frac{f_B - f_1}{\sqrt{(f_B \cdot f_1)}}. \tag{3}$$

C. Study of the Design Parameters in the Periodic Structure

The modification of the length D in the unit cell has a direct impact on the behavior of the waveguide dispersion diagram, in terms of the different modes' cutoff frequency, on one hand, and in terms of the single-mode bandwidth and prohibited bandgap position, on the other. Fig. 5 shows the dispersion diagram of the Floquet modes for different period lengths of the unit cell. As can be seen, for a step height equal to H, the fractional bandwidth Δ increases significantly by reducing the period D. This is due to the fact that by reducing D, the bandgap moves toward higher frequencies.

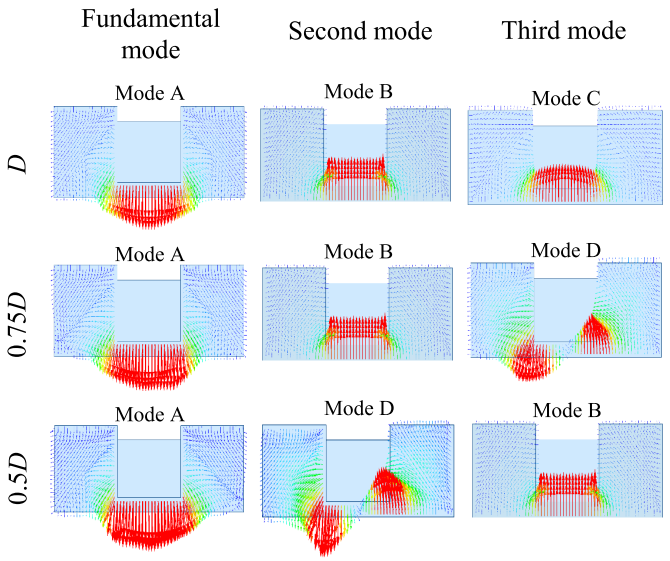

Fig. 6. Electric field distribution of the first three Floquet modes for a step height H and different period lengths of the unit cell.

TABLE I
CUTOFF FREQUENCIES OF THE FIRST TWO MODES AND BANDWIDTHS FOR A STEP HEIGHT H AND DIFFERENT PERIOD VALUES

Period length	f_1 (GHz)	f_B (GHz)	f_2 (GHz)	Δ (%)	B
D	4	4.78	9.69	17.8	1.42
0.75D	4	5.43	11.7	30.7	1.93
0.5D	4	6.8	15.6	54	2.9
0.35D	4	8.43	15.6	76.3	2.9

It can also be noted in Fig. 5 that the rejection bandwidth increases significantly as the parameter D is reduced, obtaining the maximum rejection bandwidth for $\sim 0.5D$. This is due to the fact that the first upper Floquet mode propagates at higher frequencies when the period is $0.5D$. Fig. 6 shows the electric field distribution in the central cross section of the unit cell corresponding to the first three Floquet modes for different unit cell lengths. It can be seen that the unit cell modes B and C change positions depending on the unit cell length, while the fundamental mode remains the same.

As a summary, Table I collects the cutoff frequencies of the different Floquet modes and the passband and rejection-band bandwidths for different periods of the unit cell.

On the other hand, the modification of the central section step height H also impacts directly on the Floquet modes in the structure in terms of the passband and rejection-band bandwidths. Fig. 7 shows the dispersion diagram for different values of H. It is worth mentioning that for a period $0.5D$, the passband bandwidth increases as H gets smaller.

This behavior was already explained in [10] where it was shown that when increasing the step section height in a rectangular waveguide periodic structure, the passband bandwidth increases due to a lower mode impedance contrast within the periodic cell. With regard to the rejection bandwidth (prohibited bandgap bandwidth), it gets wider as H increases. Table II shows the cutoff frequencies of the different Floquet

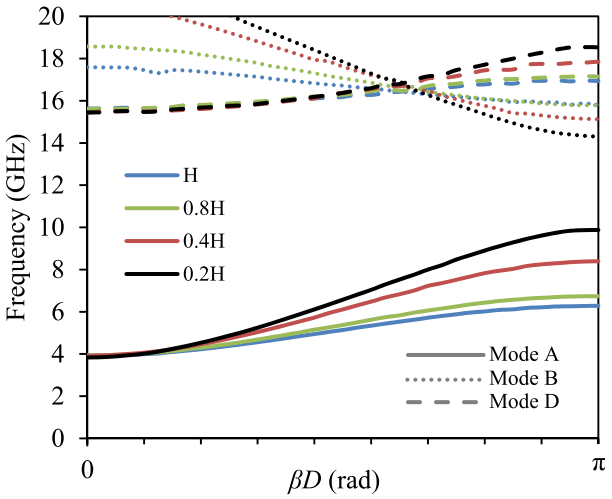

Fig. 7. Dispersion diagram of the EBG SRW for $0.5D$ and different step heights in the unit cell.

TABLE II
CUTOFF FREQUENCIES OF THE FIRST TWO MODES AND BANDWIDTHS FOR A PERIOD $0.5D$ AND DIFFERENT STEP HEIGHTS

Step height	f_1 (GHz)	f_B (GHz)	f_2 (GHz)	Δ (%)	B
H	4	6.28	15.6	45.5	2.9
0.8H	4	6.8	15.6	54	2.9
0.4H	4	8.4	15.1	75.9	2.8
0.2H	4	9.88	14.3	93.5	2.575

modes and the passband and rejection-band bandwidths for different step height H values in the unit cell.

III. FINITE SRW STRUCTURE DESIGN

Once the infinite periodic SRW structure has been studied and the effects of the design parameters (D and H) have been determined regarding f_1, B, and Δ, the finite implementation of the structure is analyzed. In this section, two filter designs with different pass-band bandwidth specifications are presented.

In these designs, two main aspects have to be accounted for. On one hand, to obtain a high rejection level in the prohibited bandgap shown in Fig. 4, a large number of unit cells (periods) must be considered [9]. However, the larger the number of periods, the longer the filter implementation. On the other hand, the Bloch impedance $Z_{0\infty}$ of the ideal periodic structure [9] differs from the fundamental mode impedance of its finite implementation [23].

It is necessary to determine the fundamental mode impedance and perform the required matching solutions to have good filter return losses in the pass-band. Fig. 8 shows an eight-unit cell finite implementation of the periodic structure of Fig. 3, where no matching element is introduced.

A. Design of a Band-Pass Filter With a Fractional Bandwidth of $\Delta = 27\%$

An SRW periodic filter with eight unit cells and $\Delta = 27\%$ at a central frequency of 4.6 GHz as shown in Fig. 9 is designed.

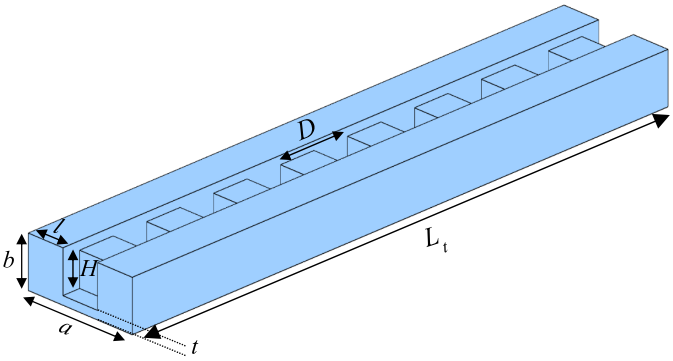

Fig. 8. Finite implementation of the EBG SRW with eight periodic cells. The dimensions indicated are as follows: $D = 7.5$mm, $H = 2.52$ mm, $a = 11.65$ mm, $b = 3.78$ mm, $t = 0.63$ mm, $l = 3.88$ mm, and $L_t = 60$ mm.

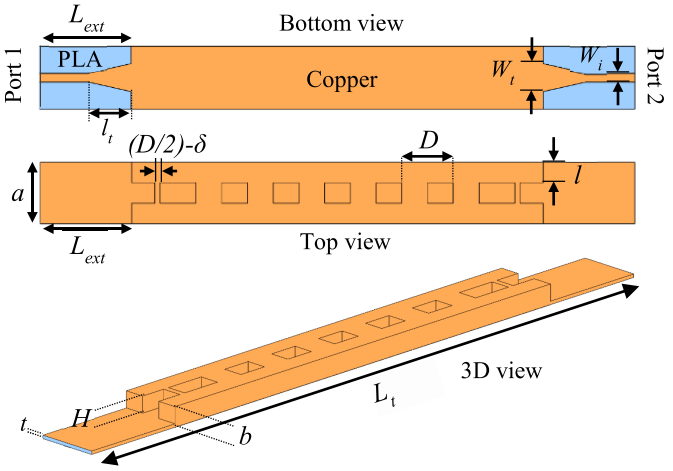

Fig. 9. Bottom view, top view, and 3-D view of the EBG SRW band-pass filter for $\Delta = 27\%$. EBG SRW filter dimensions are as follows: $D = 11.25$ mm, $H = 3.15$ mm, $a = 11.65$ mm, $b = 3.78$ mm, $t = 0.63$ mm, $l = 3.88$ mm, $\delta = 4.08$ mm, $L_{ext} = 14$ mm, $l_t = 3.88$ mm, $W_t = 5.05$ mm, $W_i = 1.6$ mm, and $L_t = 130$ mm.

The design parameters are the period length $0.75D$ (11.25 mm) and the central section step height H (3.15 mm), and they have been obtained directly using Figs. 5 and 7. A taper element is used to proceed with the matching of the structure to the 50-Ω characteristic impedance input and output microstrip lines. To calculate the width of the taper W_t on the SRW end, the fundamental mode impedance is calculated using

$$Z_0 = Z_{0\infty} \frac{1}{\sqrt{1 - \left(\frac{f_1}{f}\right)^2}} \tag{4}$$

where $f = 4.6$ GHz is the design central frequency [21].

In addition, to further improve the return losses in the passband, the first and the last periods in the finite periodic structure are modified so that their central step length measures $D/2$-δ instead of $D/2$ [10]. The simulated filter response is shown in Fig. 10 together with the cutoff frequencies of the first Floquet mode in the periodic structure.

B. Design of a Bandpass Filter With a Fractional Bandwidth of $\Delta = 54\%$

A second SRW filter, as shown in Fig. 11, is designed next with the same number of eight periodic unit cells. In this case,

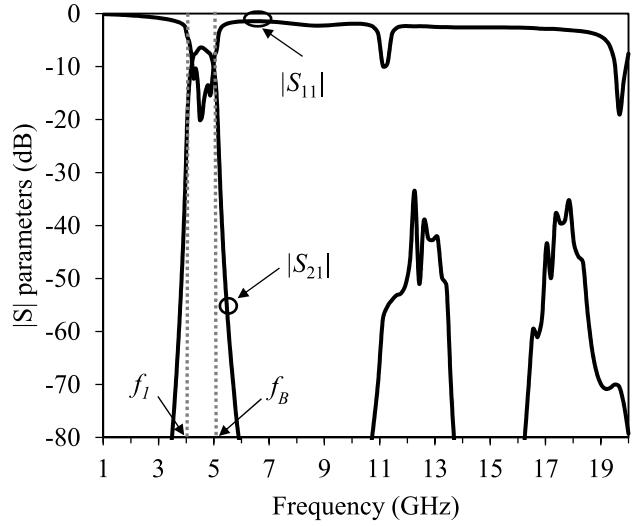

Fig. 10. Simulated scattering parameters of the $\Delta = 27\%$ filter (black lines). Also shown are the cutoff frequency of the fundamental mode and the lowest frequency of the bandgap.

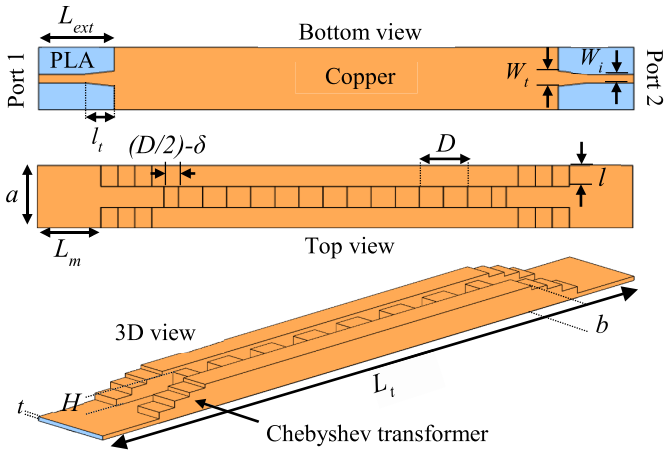

Fig. 11. Bottom view, top view, and 3D view of the EBG SRW band-pass filter for $\Delta = 54\%$. EBG SRW filter dimensions are as follows: $D = 7.5$ mm, $H = 2.52$ mm, $a = 11.65$ mm, $b = 3.78$ mm, $t = 0.63$ mm, $l = 3.88$ mm, $\delta = 1.41$ mm, $l_m = 10.26$ mm $L_{\text{ext}} = 12.26$ mm, $l_t = 4.8$ mm, $W_t = 2.85$ mm, $W_i = 1.6$ mm, and $L_t = 96.4$ mm.

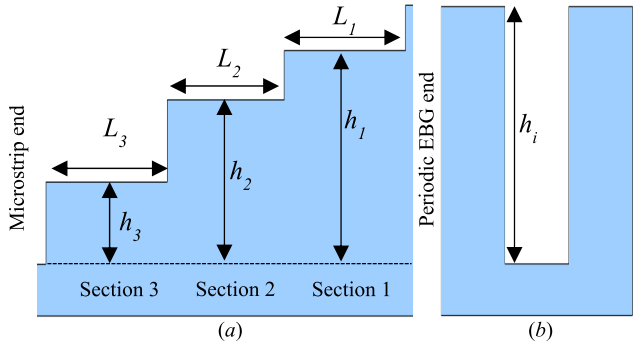

Fig. 12. Side view (a) and front view (b) of the SRW Chebyshev transformer.

the passband bandwidth has been increased up to $\Delta = 54\%$ for a central frequency of 5.4 GHz. Again, the design parameters have been determined using Figs. 5 and 7. The length of the periodic unit cell is $0.5D$ (7.5 mm), while the height of the central section step is $0.8H$ (2.52 mm).

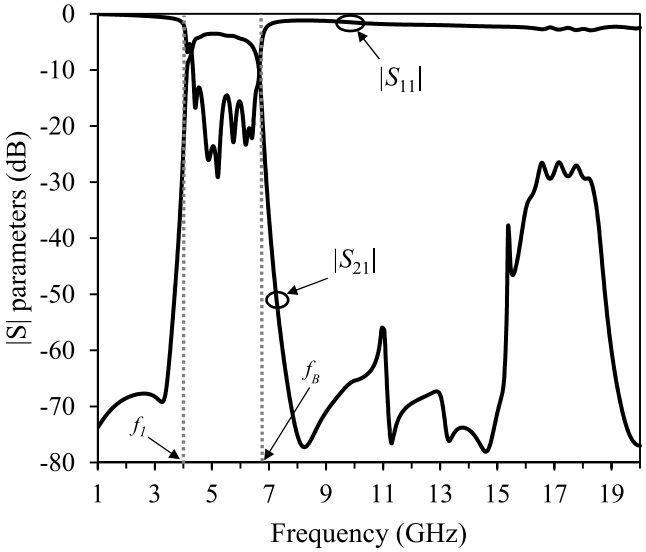

Fig. 13. Simulated scattering parameters of the $\Delta = 54\%$ filter (black lines). Also shown are the cutoff frequency of the fundamental mode and the lowest frequency of the bandgap.

As this second design presents a wider band-pass bandwidth, a single taper element is not suitable for matching purposes, so it is necessary to include a more elaborate matching solution. A three-quarter wavelength section SRW Chebyshev transformer is used to match the filter to the 50-Ω microstrip transmission lines [24]. A maximum allowable reflection coefficient magnitude of $\Gamma_m = 0.05$ is chosen for the transformer. The Bloch impedance $Z_{0\infty}$ of the infinite periodic structure is determined by means of Ansys HFSS, and the fundamental mode impedance is obtained using (4) at a central frequency of $f = 5.4$ GHz. The different fundamental mode impedances in the three sections have been synthesized changing their heights h_i as shown in Fig. 12, using the expressions [21], [23] given next

$$
\begin{aligned}
Z_{0\infty\text{SRW}} &= \frac{\pi\,\eta_0\left(\frac{t}{\lambda_{cr}}\right)}{X1 + X2} \\
X1 &= \frac{4t}{\lambda_{cr}} \ln\left(\operatorname{cosec}\left(\frac{\pi\, t}{2b}\right)\right)\cos^2(\theta_2) + \frac{\theta_2}{2} + \frac{\sin(2\theta_2)}{4} \\
X2 &= \frac{t}{b}\left(\frac{\cos(\theta_2)}{\sin(\theta_1)}\right)^2\left[\frac{\theta_1}{2} + \frac{\sin(2\theta_2)}{4}\right] \\
\theta_1 &= \frac{\pi\,(a-s)}{\lambda_{cr}} \\
\theta_2 &= \frac{\pi\, s}{\lambda_{cr}}
\end{aligned}
\tag{5}
$$

where $f_{cr} = c/\lambda_{cr}$ is the cutoff frequency of the SRW and c is the speed of light [23].

To further improve the matching of the structure, a final taper is included between the last section of the transformer and the 50-Ω microstrip transmission lines, while the length of the first and the last periods in the finite periodic structure is also modified.

Once the response of the filter is optimized, the final dimensions of the transformer sections are those as given in Table III. The simulated filter response is shown in Fig. 13 with the

TABLE III
FINAL DIMENSIONS OF THE MATCHING NETWORK SECTIONS

Section i	h_i (mm)	L_i (mm)
1	3.23	2.98
2	2.63	2.89
3	1.63	2.88

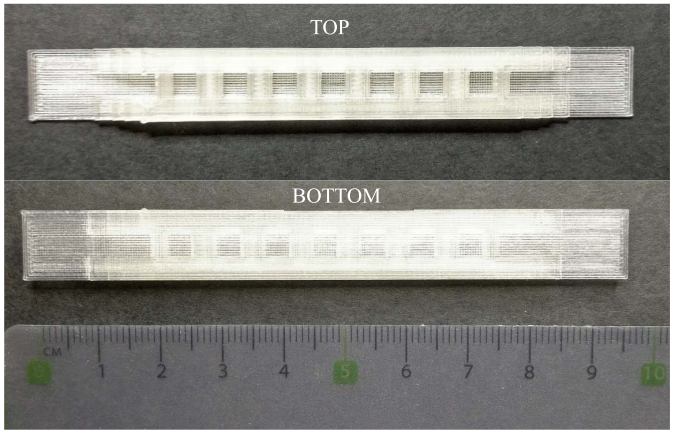

Fig. 14. Photograph of the filter printed in 3-D using PLA before the metallization process.

cutoff frequencies of the first Floquet mode in the periodic structure.

IV. EXPERIMENTAL VALIDATION

To validate the theoretical analysis given in previous sections, the 54% fractional bandwidth band-pass filter shown in Fig. 11 was fabricated and measured. A 3-D printer (3NTR A4v3) with a resolution of 15 μm in the *XY*-axis and a nozzle diameter of 300 μm along with 3-D PLA filament were used to yield the prototype as shown in Fig. 14.

The 3-D PLA filter structure produced is metallized following a two-step process. First, a conductive paint is applied to the whole surface of the structure, and second, a conventional electroplating procedure is carried out to grow the thickness of the deposited copper up to ~35 μm. Finally, an LPKF Protomat E44 milling machine is used to implement the SRW to microstrip transitions on the bottom side of the filter. Fig. 15 shows the fabricated final prototype and the Anritsu text fixture used to characterize it. Fabricated physical dimensions are within a 1% error margin from the simulated structure. The fabrication process proved to be precise and reliable. The high flexibility of 3-D printing can be exploited to improve the power handling of the component by rounding the corners of the structure.

Scattering parameter filter measurements were carried out using a Hewlett-Packard 8516A vector network analyzer. The measured S-parameters are compared with the simulated filter response in Fig. 16. The measured filter passband frequencies are $f_1 = 4.03$ GHz and $f_B = 6.8$ GHz, which are very similar to the simulated $f_1 = 4$ GHz and $f_B = 6.8$ GHz (this small deviation of the fundamental mode cutoff frequency might be due to small variations in the relative permittivity

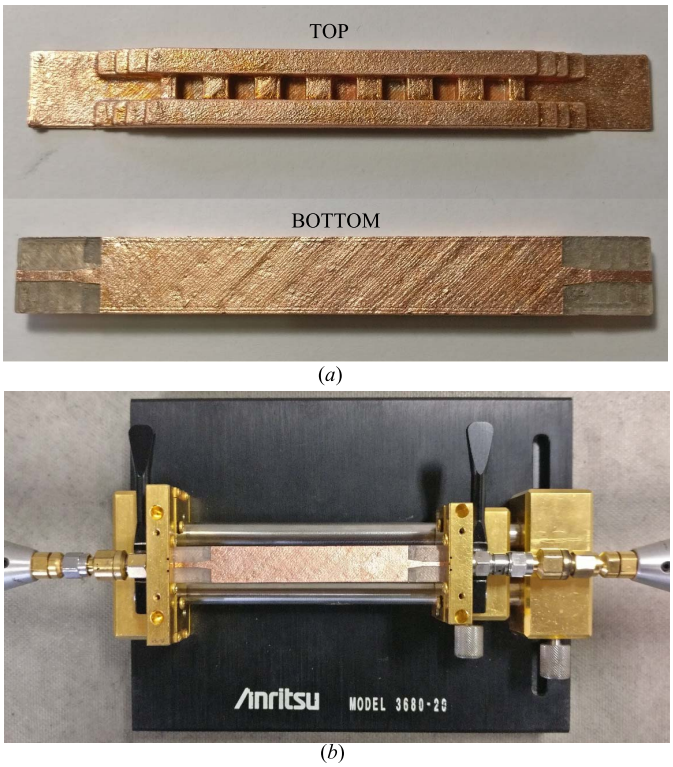

Fig. 15. (a) Photograph of the final filter prototype after the manufacturing process. (b) Measurement setup.

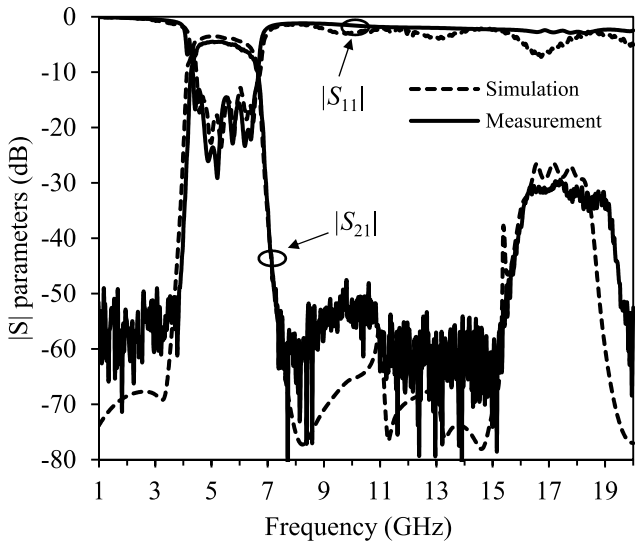

Fig. 16. Simulated and measured scattering parameters of the eight-unit cell $\Delta = 54\%$ filter as a function of frequency.

of the material and in the final filter dimensions). Simulated insertion losses within the passband are 3.5 dB, close to the 4.4-dB insertion losses obtained in measurements (this deviation might be due to the text fixture not included in the simulation). Return losses within the passband are better than 10 dB except for low frequencies, as predicted by simulations.

V. CONCLUSION

In this work, a new band-pass filter topology in waveguide technology is presented. It is based on a modified SRW structure where a periodic step height change is included in

the central section of the waveguide. A band-pass filter design process is discussed making use of the proposed topology, where the dispersion diagram of the periodic structure sets the characteristics of the filter frequency response. This process allows the full and separate control of the different filter design parameters by specific geometrical dimensions. The dispersion diagram of the periodic structure unit cell has been obtained for different design parameters, showing the ability of the designing process to provide the required passband and prohibited band frequency specifications.

To validate the proposed filter topology and designing process, two band-pass filter responses with different fractional bandwidth requirements are studied. Finally, a 54% fractional bandwidth band-pass filter prototype is fabricated using a 3-D additive manufacturing process, demonstrating the suitability and simplicity of using this type of 3-D printing implementation techniques for the proposed novel filter topology. The measured filter response is in good agreement with electromagnetic simulations and shows good passband and rejection-band performances.

The main advantages of the proposed solution are the following: The basic features of the filter frequency response (like passband and the rejection band) are defined by the simple and fast analysis of the periodic structure. The unit cell of the SRW exhibits a sufficient number of degrees of freedom, to guarantee full and separate control of the different filter design parameters by specific geometrical dimensions. The use of additive manufacturing offers large design flexibility and simple fabrication of the prototypes.

REFERENCES

[1] W. W. Gao *et al.*, "The status, challenges, and future of additive manufacturing in engineering," *Comput.-Aided Des.*, vol. 69, pp. 65–89, Dec. 2015.

[2] R. Bahr, B. Tehrani, and M. M. Tentzeris, "Exploring 3-D printing for new applications: Novel Inkjet-and 3-D-printed millimeter-wave components, interconnects, and systems," *IEEE Microw. Mag.*, vol. 19, no. 1, pp. 57–66, Jan. 2018.

[3] J. G. Hester *et al.*, "Additively manufactured nanotechnology and origami-enabled flexible microwave electronics," *Proc. IEEE*, vol. 103, no. 4, pp. 583–606, Apr. 2015.

[4] E. Massoni *et al.*, "3-D printed substrate integrated slab waveguide for single-mode bandwidth enhancement," *IEEE Microw. Wireless Compon. Lett.*, vol. 27, no. 6, pp. 536–538, Jun. 2017.

[5] F. Distler, M. Sippel, J. Schur, G. Gold, K. Helmreich, and M. Vossiek, "Additively manufactured dielectric waveguides for advanced concepts for millimeter-wave interconnects," *IEEE Trans. Microw. Theory Techn.*, vol. 67, no. 11, pp. 4298–4307, Nov. 2019.

[6] A. Vallecchi, D. Cadman, W. G. Whittow, J. Vardaxoglou, E. Shamonina, and C. J. Stevens, "3-D printed bandpass filters with coupled vertically extruded split ring resonators," *IEEE Trans. Microw. Theory Techn.*, vol. 67, no. 11, pp. 4341–4352, Nov. 2019.

[7] F. Cai, Y.-H. Chang, K. Wang, C. Zhang, B. Wang, and J. Papapolymerou, "Low-loss 3-D multilayer transmission lines and interconnects fabricated by additive manufacturing technologies," *IEEE Trans. Microw. Theory Techn.*, vol. 64, no. 10, pp. 3208–3216, Oct. 2016.

[8] G. Addamo *et al.*, "Additive manufacturing of ka-band dual-polarization waveguide components," *IEEE Trans. Microw. Theory Techn.*, vol. 66, no. 8, pp. 3589–3596, Aug. 2018.

[9] F. Martin, *Artificial Transmission Lines for RF and Microwave Applications*. Hoboken, NJ, USA: Wiley, 2015.

[10] H. García-Martínez, G. Torregrosa-Penalva, E. Ávila-Navarro, A. Coves-Soler, and E. Bronchalo, "Complex structures in microwave circuits by using additive manufacturing techniques," in *Proc. 49th Eur. Microw. Conf. (EuMC)*, Paris, France, Oct. 2019, pp. 782–785.

[11] L. Silvestri, E. Massoni, C. Tomassoni, A. Coves, M. Bozzi, and L. Perregrini, "Substrate integrated waveguide filters based on a dielectric layer with periodic perforations," *IEEE Trans. Microw. Theory Techn.*, vol. 65, no. 8, pp. 2687–2697, Aug. 2017.

[12] S. Moscato, R. Moro, M. Pasian, M. Bozzi, and L. Perregrini, "Two-material ridge substrate integrated waveguide for ultra-wideband applications," *IEEE Trans. Microw. Theory Techn.*, vol. 63, no. 10, pp. 3175–3182, Oct. 2015.

[13] D. Lopez, A. Coves, E. Bronchalo, G. Torregrosa, and M. Bozzi, "Practical design of a band-pass filter using EBG SIW technology," in *Proc. 48th Eur. Microw. Conf. (EuMC)*, Madrid, Spain, Sep. 2018, pp. 77–80.

[14] J. Helszajn, *Ridge Waveguides and Passive Microwave Components*. London, U.K.: British Library, 2000.

[15] R. Beyer, F. Arndt, and W. Hauth, "Modal block LU-decomposition technique for the efficient CAD of ridged waveguide filters," in *IEEE MTT-S Int. Microw. Symp. Dig.*, Jun. 1997, pp. 1235–1238.

[16] S. Li, J. Fu, and X. Wu, "Double-ridged waveguide low-pass filters for satellite application," in *Proc. IEEE Int. Symp. Microw. Antennas, Propag. (EMC)*, Aug. 2007, pp. 408–410.

[17] M. Bozzi, S. A. Winkler, and K. Wu, "Broadband and compact ridge substrate-integrated waveguides," *IET Microw., Antennas Propag.*, vol. 4, no. 11, pp. 1965–1973, Nov. 2010.

[18] Á. Coves, S. Marini, B. Gimeno, and V. Boria, "Full-wave analysis of periodic dielectric frequency-selective surfaces under plane wave excitation," *IEEE Trans. Antennas Propag.*, vol. 60, no. 6, pp. 2760–2769, Jun. 2012.

[19] S. J. Lavdas, C. S. Lavranos, and G. A. Kyriacou, "Periodic structures eigenanalysis incorporating the floquet field expansion," in *Proc. Int. Conf. Electromagn. Adv. Appl.*, Turin, Italy, Sep. 2011, pp. 1253–1256.

[20] T. K. Mealy, I. A. Eshrah, and T. M. Abuelfadl, "Solution of periodically loaded waveguides using the eigenmode projection technique," in *IEEE MTT-S Int. Microw. Symp. Dig.*, San Francisco, CA, USA, May 2016, pp. 1–4.

[21] S. Hopfer, "The design of ridged waveguides," *IEEE Trans. Microw. Theory Techn.*, vol. MTT-3, no. 5, pp. 20–29, Oct. 1955.

[22] H. García-Martínez, E. Ávila-Navarro, G. Torregrosa-Penalva, A. Rodriguez-Martínez, and M. de la Casa-Lillo, "Analysis of microwave passive circuits designed using 3D printing techniques," *Elektronika Elektrotechnika*, vol. 25, no. 2, pp. 36–39, Apr. 2019.

[23] W. J. R. Hoefer and M. N. Burton, "Closed-form expressions for the parameters of finned and ridged waveguides," *IEEE Trans. Microw. Theory Techn.*, vol. 30, no. 12, pp. 2190–2194, Dec. 1982.

[24] D. M. Pozar, *Microwave Engineering*. New York, NY, USA: Wiley, 1998.

Héctor García-Martínez was born in Albatera, Spain, in 1991. He received the master's degree in telecommunication engineering from the University Miguel Hernández of Elche, Elche, Spain, in 2016.

He was a Visiting Scholar with the University of Pavia, Pavia, Italy, in 2019. He is currently an Associate Professor at the Department of Materials Science, Optics and Electronic Technology, and a Researcher with the Radiofrequency System Group, University Miguel Hernandez of Elche. His research interests include the design of passive and active microwave circuits in complex structures through 3-D additive manufacturing techniques and the analysis of biological materials using microwave devices.

Ernesto Ávila-Navarro received the M.Sc. degree in telecommunication engineering from the Polytechnic University of Valencia, Valencia, Spain, in 1998, and the Ph.D. degree from the Miguel Hernández University of Elche, Elche, Spain, in 2008, for a work on planar antennas for specific personal wireless applications.

In 2000, he joined the University Miguel Hernández of Elche, where he is currently an Associate Professor with the Electronic Technology Department. Currently, he is a Vice Dean of the High Polytechnic School of Engineering of Elche, Elche. His current research interest includes printed antennas, passive and active microwave devices, bioelectronics, and microwave imaging systems for cancer detection.

Germán Torregrosa-Penalva (Member, IEEE) received the telecommunications engineering and Ph.D. degrees from the Universidad Politécnica de Madrid (UPM), Madrid, Spain, in 1999 and 2004, respectively.

In October 2002, he joined the Signal Theory and Communications Division, Miguel Hernández University of Elche, Elche, Spain, where he is currently an Associate Professor. His research interests include the study of electron discharges in microwave components, sensor networks using microwave photonics, thermal and electrical characterization of microwave power amplifiers, additive manufacturing of high-frequency devices, and the design of microwave circuits and subsystems.

Nicolò Delmonte (Student Member, IEEE) was born in Broni, Italy, in 1992. He received the B.S. degree in electronics and computer engineering and the M.S. degree in electronic engineering from the University of Pavia, Pavia, Italy, in 2015 and 2017, respectively, where he is currently pursuing the Ph.D. degree in electronic engineering at the Microwave Laboratory.

His research interests include passive microwave components, substrate integrated waveguide (SIW) structures, and phased array design. Mr. Delmonte was a recipient of the IEEE MTT-S undergraduate scholarship in 2015.

Lorenzo Silvestri (Member, IEEE) was born in Novara, Italy, in 1987. He received the master's degree in electronic engineering and the Ph.D. degree in electronics, computer science, and electrical engineering from the University of Pavia, Pavia, Italy, in 2014 and 2019, respectively.

In 2014, he was recipient of a one-year post-graduate scholarship at the University of Pavia, working on passive substrate integrated waveguide (SIW) components. He was a Visiting Scientist at Ghent University, Ghent, Belgium, and Université de Bordeaux, Bordeaux, France. He currently holds a post-doctoral position at the Microwave Laboratory, University of Pavia, where his main research interests are related to the development of new components based on SIW technology on innovative substrate materials.

Dr. Silvestri was a recipient of the Best Paper Award at the 15th Mediterranean Microwave Symposium (MMS2015).

Stefania Marconi received the master's degree in biomedical engineering and the Ph.D. degree in experimental surgery and microsurgery from the University of Pavia, Pavia, Italy, in 2011 and 2015, respectively.

She is currently an Assistant Professor at the University of Pavia and she coordinates the research activity of 3D4Med (www.3d4med.eu), the Clinical 3-D printing laboratory of IRCCS Policlinico San Matteo, Pavia. She has authored about 50 works on referred international journals and 2 patents. Her research activity is focused on 3-D printing technologies and materials, especially for medical application.

Gianluca Alaimo was born in Palermo, Italy, in 1976. He received the master's degree in mechanical engineering, the master's degree in biomechanical engineering, and the Ph.D. degree in civil engineering from the University of Palermo, Pavia, Italy, in 2012, 2013, and 2018, respectively.

He is currently a Post-Doctoral Fellow at the University of Pavia, Pavia, where he is also jointly responsible of the 3-D printing laboratory. His research interest actually covers additive manufacturing with the related new materials and printing technologies, optimization techniques, and numerical simulation of manufacturing processes.

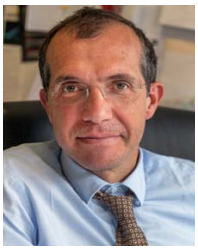

Ferdinando Auricchio is currently a Professor of solids and structural mechanics with the Department of Civil Engineering and Architecture, University of Pavia, Pavia, Italy, and a Research Associate at Institute for Applied Mathematics and Information Technologies of the National Research Council (IMATI-CNR), Pavia.

Mr. Auricchio received the Euler Medal by European Community of Computational Methods in Applied Sciences (ECCOMAS) in 2016 and the Fellow Award by International Association for Computational Mechanics (IACM) since 2012. From 2013 to 2019, he served as a Vice President of ECCOMAS. In 2018, he was appointed as a member of the Italian National Academy of Science, known also as Accademia dei XL.

Maurizio Bozzi (Fellow, IEEE) received the Ph.D. degree in electronics and computer science from the University of Pavia, Pavia, Italy, in 2000.

In 2002, he joined the Department of Electronics, University of Pavia, where he is currently a Full Professor of electromagnetic fields. He held research positions with various universities worldwide, including the Technische Universität Darmstadt, Darmstadt, Germany; the Universitat de Valencia, Valencia, Spain; and the École Polytechnique de Montréal, Montréal, QC, Canada. He was also a Guest Professor at Tianjin University, Tianjin, China, from 2015 to 2017, and a Visiting Professor at Gdansk University of Technology, Gdansk, Poland, from 2017 to 2018. He has authored or coauthored more than 140 journal articles and 330 conference articles. He co-edited the book *Periodic Structures* (Research Signpost, 2006) and coauthored the book *Microstrip Lines and Slotlines* (Artech House, 2013). His main research interests concern the computational electromagnetics, the substrate integrated waveguide technology, and the use of novel materials and fabrication technologies for microwave circuits.

Dr. Bozzi is an Elected Member of the Administrative Committee of the IEEE Microwave Theory and Techniques Society (MTT-S) from 2017 to 2022 and the MTT-S Treasurer in 2020. He was the Chair of the Meetings and Symposia Committee of MTT-S AdCom from 2018 to 2019, the Secretary of IEEE MTT-S in 2016, and a member of the General Assembly (GA) of the European Microwave Association (EuMA) from 2014 to 2016. He is a Track Editor of the IEEE TRANSACTIONS ON MICROWAVE THEORY AND TECHNIQUES. He was an Associate Editor of the IEEE MICROWAVE AND WIRELESS COMPONENTS LETTERS, the *IET Electronics Letters*, and the *IET Microwaves, Antennas and Propagation*. He was the Guest Editor of special issues in the IEEE TRANSACTIONS ON MICROWAVE THEORY AND TECHNIQUES, IEEE *Microwave Magazine*, and the *IET Microwaves, Antennas and Propagation*. He was the General Chair of the IEEE MTT-S International Microwave Workshop Series-Advanced Materials and Processes (IMWS-AMP 2017), in Pavia, Italy, 2017, the inaugural edition of the IEEE International Conference on Numerical Electromagnetic Modeling and Optimization (NEMO2014), in Pavia, Italy, 2014, and the IEEE MTT-S International Microwave Workshop Series on Millimeter Wave Integration Technologies, in Sitges, Spain, 2011. He received several awards, including the 2015 Premium Award for Best Paper in IET Microwaves, Antennas and Propagation, the 2014 Premium Award for the Best Paper in Electronics Letters, the Best Student Paper Award at the 2016 IEEE Topical Conference on Wireless Sensors and Sensor Networks (WiSNet2016), the Best Paper Award at the 15th Mediterranean Microwave Symposium (MMS2015), the Best Student Award at the 4th European Conference on Antennas and Propagation (EuCAP 2010), the Best Young Scientist Paper Award of the XXVII General Assembly of URSI in 2002, and the MECSA Prize of the Italian Conference on Electromagnetics (XIII RiNEm), in 2000.